Theoret. Comput. Fluid Dynamics (2004) 17: 165–170
Digital Object Identifier (DOI) 10.1007/s00162-003-0101-5

Theoretical and Computational Fluid Dynamics

Flutter, Tumble and Vortex Induced Autorotation

Rajat Mittal and Veeraraghavan Seshadri

Department of Mechanical and Aerospace Engineering,
The George Washington University,
Washington, DC 20052, U.S.A.

Holavanahalli S. Udaykumar

Department of Mechanical Engineering,
University of Iowa,
Iowa City, IA 52242, U.S.A.

Communicated by M.Y. Hussaini

Received 6 August 2003 and accepted 12 September 2003
Published online 16 January 2004 – © Springer-Verlag 2004

Abstract. The phenomenon of flutter and tumble of objects in free fall has been studied using two-dimensional numerical simulations of uniform flow past a plate which is free to rotate about a fixed axis through its centroid. Particular focus is on the effect of Reynolds number and plate thickness-to-length ratio on the flutter-to-tumble transition and on the observed frequency of the angular motions. Simulations indicate that the tendency to tumble increases with increasing Reynolds number and decreasing thickness ratio. A case is also made that the tumbling frequency for two-dimensional plates is governed by a Karman type vortex shedding process. These results for this pinned plate have also been verified by simulating a limited number of free-fall cases.

The motion of objects falling in a fluid has been of interest to physicists since at least the time when Maxwell first examined the motion of falling paper in 1854 [1]. The phenomenon exhibits rich physics with a number of regimes of motion including periodic or chaotic side-to-side motion ("flutter") and end-over-end rotation ("tumble"). The motion of falling objects is also of direct relevance in areas as diverse as the functional morphology of plants and animals [2], meteorology and aeroballistics [3]. Recently there has been a surge of interest in this problem [4]–[7], and resulting studies have greatly increased our understanding of this phenomenon. However, it is fair to say that many important aspects of this phenomenon are still not well understood. In particular, there is relatively little insight into the role that vortex shedding plays on the motion of falling objects. The fluid dynamics associated with these shed vortices as well as its subsequent effect on the motion of the object can be complex enough to make theoretical treatment difficult. Experiments and numerical simulations then provide the primary means of examining these flow problems.

To put this problem into perspective, consider the motion of a freely falling rectangular plate or circular disk which is governed by the following parameters: Reynolds number $Re = V_0 L/\nu$, where V_0 is the mean terminal velocity, L is the length (or diameter) of the plate and ν the kinematic viscosity of the fluid; plate thickness ratio $\tau = t/L$, where t is the plate thickness; and a non-dimensional moment of inertia $I^* = I/\left(\varrho_{\mathrm{f}} L^4 w\right)$ [8], where w is the plate width ($= L$ for the circular disk), ϱ_{f} is the fluid density and I is the

moment of inertia of the plate about the axis of rotation. For rotation about the plate center axis aligned with the width, one gets I^* equal to $\frac{1}{12}\,(\varrho_s/\varrho_f)\,\tau$ and $(\pi/64)\,(\varrho_s/\varrho_f)\,\tau$ for rectangular plates and circular disks respectively where ϱ_s is the density of the solid plate. For rectangular plates, the plate aspect ratio (w/L) is an additional parameter but for large aspect-ratio plates this parameter effectively drops out from the problem. Thus, for circular or large aspect-ratio rectangular plates, the motion in free fall, and, in particular, the transition from flutter to tumble, should be completely governed by the three parameters Re, τ and I^*.

Field *et al.* [5] made comprehensive measurements of the motion of circular disks and mapped out the various regimes of motion that were observed. In their experiment they kept $\tau \ll 1$ and varied Reynolds number from about 20 to 3×10^4 and I^* from 3×10^{-4} to 0.2. They found that tumbling occurred for $I^* \gtrapprox 0.04$ and $Re \gtrapprox 200$. Belmonte *et al.* [4] on the other hand, examined the motion of rectangular flat plates in a Hele–Shaw type apparatus. In their experiments, Reynolds numbers were greater than 3×10^3 and the thickness ratio was kept below a value of 0.2. The primary focus was to correlate the flutter-to-tumble transition to the Froude number which was defined as $Fr = \left(M/\varrho_f L^2 w\right)^{1/2}$ and the plates were found to transition from flutter to tumble at $Fr \approx 0.67$. Interestingly, for rectangular plates, $I^* = \frac{1}{12} Fr^2$ and, therefore, the experiments in [4] predict a critical value of I^* of 0.037 which is almost identical to that predicted in [5]. Willmarth *et al.* [8] have also studied freely falling disks and note that the transition to tumbling occurred at values of $I^* \gtrapprox 0.01$. Finally, Iverson [9] analyzed experimental data for freely falling rectangular plates and found a sudden and significant increase in the tip-speed, indicative of the flutter-to-tumble transition, at around $I^* = 0.05$.

The dependence of the flutter-to-tumble transition on I^* is therefore quite well established and the critical value of this parameter seems to be quite insensitive to the other parameters. On the other hand, the effect of the thickness ratio τ and the Reynolds number Re on this transition is relatively less well understood and the objective of the current study is to use numerical simulations to examine the role of these parameters on the transition process. We focus here on the lower $\left(\sim 10^2\right)$ Reynolds number regime where vortex shedding and the resulting motion is expected to be quite sensitive to this parameter.

Numerical simulation of freely falling objects is difficult since in general, this requires simulating flow with moving solid boundaries. Additional requirements of large integration times and computational domains can substantially increase the computational expense of these simulations and make a comprehensive analysis difficult. In the current study the above difficulties are minimized by choosing a simpler configuration which models many of the features of the freely falling object. This configuration consists of a two-dimensional flat plate with rounded tips with tip-to-tip length L and thickness t, which is exposed to a freestream with velocity V_0 and is free to rotate about a frictionless pin through its center axis which is perpendicular to the freestream. The rotational motion of this plate is also governed by the three parameters Re, τ and I^*. Depending on the values of these parameters, the plate is expected either to exhibit angular oscillations or a rotation (termed "autorotation") and these motions are expected to be analogous to flutter and tumble respectively for the same plate in free fall. Experimental observations [4], [5] suggest that for cases where the plate executes either a tumbling or a small amplitude flutter motion, the similarity to a flow past a pinned plate would be quite good. A particularly strong case for this similarity has been made by Iverson [9] in his paper. Further support for this comes from Lugt [10] who predicts a critical value of I^* of about 0.06 for autorotation which is in line with that of tumble of freely falling bodies. The use of this simpler configuration eases the computational requirements and allows us to perform a large number of simulations. Furthermore, the pinned plate configuration allows us to control the Reynolds number quite precisely which is one key control parameter in this study. Since the other parameter of interest here is the thickness ratio τ, the value of the parameter I^* is kept greater than 0.17 for all the cases studied here and this effectively removes the sensitivity of the results to this parameter. This insensitivity has been confirmed by recomputing many of the cases with higher values of I^*.

A two-dimensional, unsteady, viscous incompressible flow solver is employed which allows us to solve flow past complex moving bodies on stationary Cartesian grids. The governing equations therefore are

$$\frac{\partial u_i}{\partial x_i} = 0, \qquad \frac{\partial u_i}{\partial t} + \frac{\partial (u_i u_j)}{\partial x_j} = -\frac{\partial p}{\partial x_i} + \frac{1}{Re}\frac{\partial^2 u_i}{\partial x_j\,\partial x_j}, \tag{1}$$

where $i = 1, 2$ and u and p are the velocity and pressure respectively. The simulation methodology and the accuracy and fidelity of the flow solver has been described in detail previously [11]. A 162×162

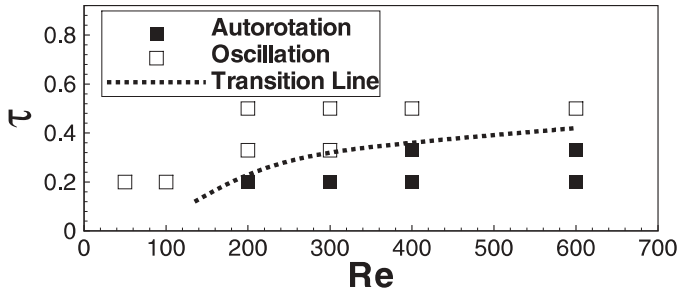

Figure 1. Phase plot showing region of transition from flutter to autorotation for the pinned plate. I^* is equal to 0.17 which is higher than the critical value.

non-uniform Cartesian mesh has been used in the current study where high resolution is provided to the region around the plate and in the wake. A large domain of size $62L \times 62L$ has been used and we apply uniform inlet velocity conditions at the bottom, left and right boundaries and a convective boundary condition on the top exit boundary which allows the vortices to exit the domain without any significant reflections. The time step ($\Delta t(V_0/L)$) employed is less than 0.005 for all cases simulated here. In addition to the flow equations we time-advance the equation $\ddot{\theta} = M_h/I$ for the plate motion at each time step and update the location of the plate surface. Note that $\ddot{\theta}$ is the angular acceleration of the plate and M_h is the hydrodynamic moment on the plate. A series of simulations of flow past the pinned plate have been carried out at Reynolds numbers of 50, 100, 200, 300, 400 and 600 and thickness ratios of $\frac{1}{2}$, $\frac{1}{3}$ and $\frac{1}{5}$. We have also carried out simulations of the forced rotation of the $\left(\tau = \frac{1}{3}\right)$ plate at the highest Reynolds number of 600 on two different grids (162×162 nominal grid and finer grid with 50% more resolution in both direction) as well as two different domains ($62L \times 62L$ nominal domain and $93L \times 93L$ larger domain). For these simulations key quantities such as mean and root-mean-square lift, drag and moment coefficients are found to vary by less than 3% from their nominal values and this establishes the numerical accuracy of these simulations. Note that in this study we simulate over 14 cycles of oscillation/rotation which allows us to base our results on a large sample in the stationary regime of the flow.

The τ versus Re "phase" plot in Figure 1 summarizes the results obtained from our simulations. In this plot, filled and open squares indicate autorotating and fluttering cases respectively, and the dashed line demarcates the boundary between these two regimes. The plot suggests that there is a minimum Reynolds number between 100 and 200 below which the plate would not autorotate for any thickness ratio. This is in line with the observation of Field *et al.* [5] for freely falling circular plates where they also found that a minimum Reynolds number value of about 200 was required for tumbling to occur. It is also clear that as the thickness ratio increases, the transition to autorotation is found to occur at increasingly higher values of Reynolds numbers. As expected the observed trend suggests that as $\tau \to 1$ (i.e. we approach the shape of a circular cylinder) the plate would not autorotate for any value of Reynolds number. In fact, the trend in the data suggest that this condition may be attained at values of τ as low as 0.6 for the plate considered in the current study.

To examine this behavior further, consider three cases. First is the case for which $Re = 200$ and $\tau = \frac{1}{3}$ where autorotation is not observed. Figure 2(a) shows a spanwise vorticity contour plot at one time instant for this case and this shows the presence of Karman vortex shedding in the wake of this plate. The second case chosen is this same plate at $Re = 400$ where autorotation is observed and Figure 2(b) shows the vorticity contour plot for this case. The final case chosen is the $Re = 400$; $\tau = \frac{1}{2}$ case which does not autorotate and it vorticity contours are shown in Figure 2(c). Comparison of the first two cases reinforces the notion [4] that even for thin plates, the mere presence of vortex shedding does not necessarily lead to autorotation. On the other hand, comparison of the second and third cases shows that even in the presence of relatively high Reynolds number vortex shedding, thick plates tend to resist autorotation. The task now is to explain these observed trends in terms of flow physics.

The current simulations indicate that plate rotation is a result of the oscillatory moment produced on the plate due to vortex shedding. With increasing moment amplitude, the amplitude of the angular oscillation also increases giving way eventually to autorotation. The key then is to explain why reduction in τ

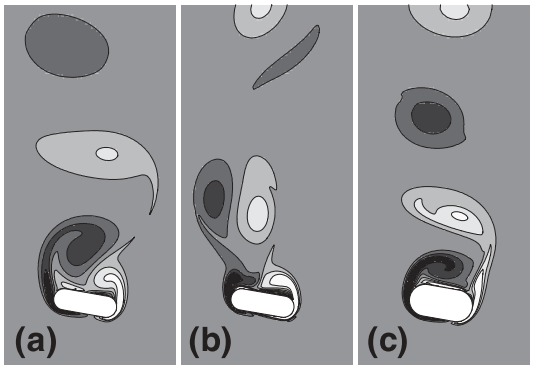

Figure 2. Plots of instantaneous spanwise vorticity for flow past the pinned plate. Freestream is directed upwards. (a) $\tau = \frac{1}{3}$; $Re = 200$; flutter. (b) $\tau = \frac{1}{3}$; $Re = 400$; autorotation. (c) $\tau = \frac{1}{2}$; $Re = 400$; flutter.

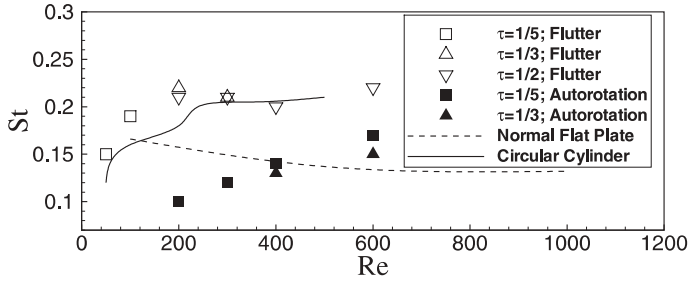

Figure 3. Variation of Strouhal number with Reynolds number for various cases.

and increase in Re would tend to increase the moment amplitude. We put forth a simple explanation for this behavior. First, computations show that most of the moment is produced due to the surface pressure and not the shear stress. This is so because shear stress levels are relatively low at these Reynolds numbers and also because the average moment arm for shear stress is smaller than that for pressure. Second, it appears that the moment on the plate is produced primarily by low pressure on the leeward side of the plate due to the shedding of vortices. Now consider that the presence of a vortex near one of the tips of the plate in the lee side of the plate produces a uniform suction pressure on one-half of the plate surface extending from the plate center to the tip of the plate where the vortex is located. For the plate with rounded tips, it can be shown that this uniform pressure distribution will produce a moment which is proportional to $(1 - \tau)$. Thus, decreasing values of τ should increase the tendency of the plate to autorotate. Now obviously, the pressure distribution due to vortex shedding is not uniform. In fact, as the Reynolds number increases, the vortices that roll up tend to be of higher strength, are more compact and roll up closer to the tip of the plate. Thus, as the Reynolds number increases, the magnitude of the suction pressure increases, and, furthermore, this higher suction acts closer to the plate tip. This results in a higher moment and consequently an increased tendency towards autorotation. Our interpretation regarding the effect of the thickness ratio is therefore somewhat different from that of Lugt [10] who suggested that sharper tips (associated with low values of τ) lead to intensification of vorticity and therefore to an increased tendency to autorotate.

It should be pointed out that the dependence of the transition on the thickness ratio is expected to be shape dependent. For instance, for a plate with squared tips, the moment coefficient would not depend on the plate thickness ratio and therefore the tendency to autorotate should be relatively insensitive to this parameter. This is indeed the case as shown by Skews [12] who found that such plates autorotate quite easily even when $\tau = 1$ (i.e. when they have square cross section).

In addition to the flutter-to-tumble transition, the current simulations also allow us to examine the scaling of the flutter/tumble frequency. Figure 3 shows the Strouhal frequency ($\mathrm{St} = \Omega L/V_0$, where Ω is the flutter or autorotation frequency obtained from examining the temporal variation of the plate angle) plotted against the Reynolds number. Also plotted here is the variation of the vortex shedding Strouhal frequency for

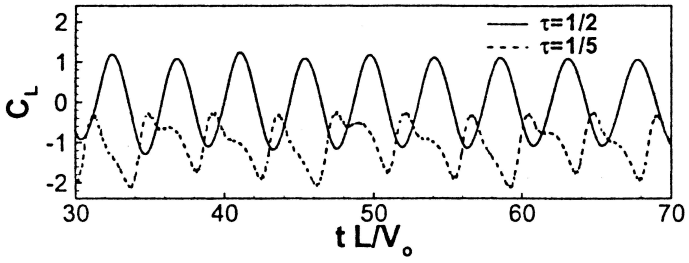

Figure 4. Variation of lift coefficient for a flutter and autorotation case at $Re = 300$.

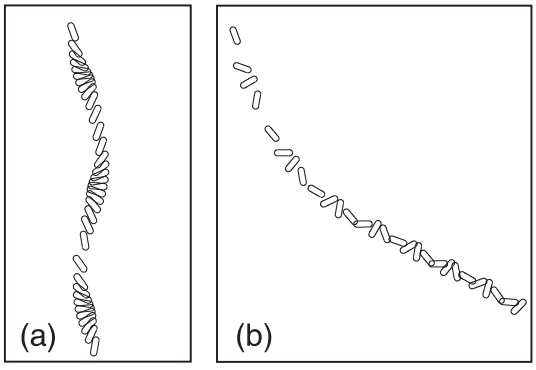

Figure 5. Motion of the $\tau = \frac{1}{3}$ plate in free fall. (a) $Re \approx 200$, (b) $Re \approx 410$.

a two-dimensional, normal fixed plate [13] and a circular cylinder [14]. Note that the former is a computational study whereas the latter is experimental. It is evident from this plot that the flutter frequency is in reasonable agreement with the Strouhal frequency of these bluff bodies. This is expected since for low amplitude flutter, the vortex shedding from the pinned plate is expected to be quite similar to that observed for these bluff bodies. Interestingly, even the frequency for the autorotating cases is in reasonable agreement with the observed frequencies for the normal flat plate. This strongly suggests that the autorotation/tumbling frequency is primarily determined by the Karman vortex shedding process. It should be noted that for lower aspect-ratio plates, the aspect ratio is also known to affect this frequency [6]. However, it is interesting to point out that even for plates with aspect ratio (w/L) as low as 10/6 and Reynolds numbers as high as $O(10^4)$, the Strouhal number is found to be about 0.15 [12] which suggests that the connection between vortex shedding and autorotation is quite robust.

Figure 4 is shows the variation of the lift coefficient for a flutter case at $Re = 300$ for which $\tau = \frac{1}{2}$ and an autorotation case at this Reynolds number which corresponds to $\tau = \frac{1}{5}$. Within sampling error, the flutter case experiences a zero mean lift whereas the autorotating plate experiences a non-zero mean lift with coefficient equal to about -1.1 for this case. The mean C_L value is in the 1.0–1.5 range for all the autorotating cases simulated here and this is very much in line with the measurement of Skews [12]. The generation of mean lift is associated with the well-know Magnus effect [15] and this has implications for the development of dynamical models of freely falling bodies [4], [7], [16]. Note that the negative value of lift is consistent with the counterclockwise rotation of the flat plate.

In order to demonstrate further that the pinned plate results have a direct bearing on the dynamics of freely falling plates, a limited number of simulations of freely falling plates have also been carried out for the $\tau = \frac{1}{3}$ plate. These simulations employ a 982×982 mesh and are substantially more CPU intensive than the pinned plate computations. In these simulations, we also solve $m\ddot{\mathbf{x}} = \mathbf{F}_\mathrm{h} + \mathbf{F}_\mathrm{g}$ for the acceleration of the plate where m and $\ddot{\mathbf{x}}$ are the plate mass and acceleration respectively, and $\mathbf{F}_\mathrm{h}$ and $\mathbf{F}_\mathrm{g}$ are the hydrodynamic and gravitational forces respectively. Four simulations with different fluid viscosities were carried out. Once the transients in the motion died out, the mean terminal velocity of each plate was computed and from this, an *a posteriori* estimate of the Reynolds number obtained. Figure 5(a) shows the snapshots for the case where

$Re \approx 200$ and this case is found to exhibit flutter. Figure 5(b) shows the snapshots for the $Re \approx 410$ case which is found to exhibit classic tumbling type motion. This observed behavior is very much in line with that found for the pinned plate shown in Figure 1. The two other free-fall cases simulated also exhibit behavior consistent with Figure 1.

The current simulations therefore show that in the range of parameters studied here, the transition from flutter to tumble for freely falling plates depends significantly on the thickness ratio and the terminal velocity Reynolds number. The simulations suggest a simple physical explanation for this dependence and also allow us to hypothesize the effect that change in the cross-sectional shape of the plate would have on this transition. Based on our results, we suggest that the flutter and tumble frequency of large aspect-ratio plates is governed by the Karman vortex shedding process. For $Re \gtrapprox 200$ the flow is expected to become three-dimensional and that could introduce additional complexities. These effects are missing from the current two-dimensional simulations and three-dimensional simulations are being initiated to explore these complexities.

References

[1] Maxwell, J.C. (1890). *Scientific Papers of James Clerk Maxwell*. pp. 115–118. Dover, New York.
[2] Azuma, A. (1992). *The Biokinetics of Flying and Swimming*. Springer-Verlag, Tokyo.
[3] Lugt, H.J. (1983). *Ann. Rev. Fluid Mech.*, **15**, 123–147.
[4] Belmonte, A., Eisenberg, H., and Moses, E. (1998). *Phys. Rev. Lett.*, **81**(2), 345–348.
[5] Field, S.B., Klaus, M., Moore, M.G., and Nori, F. (1997). *Nature*, **388**, 252–254.
[6] Mahadevan, L., Ryu, W.S., and Samuel, A.D.T. (1999). *Phys. Fluids*, **11**(1), 1–3.
[7] Tanabe, Y., and Kaneko, K. (1998). *Phys. Rev. Lett.*, **73**(2), 1372–1375.
[8] Willmarth, W.W., Hawk, N.E., and Harvey, R.L. (1994). *Phys. Fluids*, **7**(2), 197–208.
[9] Iverson, J.D. (1979). *J. Fluid Mech.*, **92**(2), 327–348.
[10] Lugt, H.J. (1980). *J. Fluid Mech.*, **99**(4), 817–840.
[11] Udaykumar, H. S., Mittal, R., Rampunggoon, P., and Khanna, A. (2001). *J. Comp. Phys.*, **174**, 245–380.
[12] Skews, B.W. (1990). *J. Fluid Mech.*, **217**, 33–40.
[13] Najjar, F.M., and Vanka, S.P. (1995). *Int. J. Numer. Meth. Fluids*, **21**, 525–547.
[14] Williamson, C.H.K. (1996). *Ann. Rev. Fluid Mech.*, **28**, 477.
[15] Batchelor, G.K. (1967). *An Introduction to Fluid Dynamics*. Cambridge University Press, Cambridge (1967).
[16] Aref, H., and Jones, S.W. (1993). *Phys. Fluids*, **A(5)**, 12, 3026.